

Enhanced Low-Voltage Ride-Through Control Strategy of Grid-Forming Converter Based on Virtual Synchronous Generator

Feng. Ji^{1*}, Zhuang. Xu²

¹ Faculty of Science and Engineering, University of Nottingham Ningbo China

² Key Laboratory of More Electric Aircraft Technology of Zhejiang Province, University of Nottingham Ningbo China

ABSTRACT

The characteristics of synchronous generator can be emulated by power electronic devices to provide moment of inertia and damping for the power grid. It is considered an effective way to connect sustainable energy generation to the power grid. If the voltage of grid-connection point drops because of power grid failure, it may lead to overcurrent, unbalance and instability for virtual synchronous generator (VSG). Therefore, a low-voltage ride-through (LVRT) control strategy for VSG is proposed in the paper. The power loop of VSG is analyzed based on the small-signal model. When an asymmetric fault occurs in the power grid, the positive and negative sequence current control is performed to achieve output current balance. The transient and steady current can be restrained by extra virtual reactance. At the same time, the reactive power is increased to support power grid voltage and the active power is decreased to restrain the steady current and improve the stability. The simulation and experimental results show that the control strategy is effective.

Keywords: Virtual Synchronous Generator, Small Signal Model, Low-voltage Ride-through, Power Loop

TABLE 1: NOMENCLATURE

Symbol	Description
I_{ld_n}	Negative Sequence D-axis Current
I_{lq_n}	Negative Sequence Q-axis Current
U_{od_n}	Negative Sequence D-axis Voltage

U_{oq_n}	Negative Sequence Q-axis Voltage
ωL_{f1}	D-axis Compensation Inductance
U_{abc-}	Three-phase Negative Sequence Voltage
ωL_{f2}	Q-axis Compensation Inductance
ωt	Electrical Angle
ω	Angular Frequency
ω_0	Initial Angular Frequency
U_{β}	Input of Second Order Generalized Integrator

1. INTRODUCTION

With the rapid development of distributed power generation, a number of problems have been exposed such as three-phase unbalance because of harmonics. It is also easily affected by meteorological factors which cannot guarantee the stability for microgrid. Though the conventional grid-connected inverters can respond quickly, there is almost no moment of inertia and damping which is difficult to participate in voltage and frequency regulation. Therefore, VSG is proposed to the converter control which can emulate synchronous generator characteristics. It can not only take part in the frequency and voltage regulation, but also enhance the stability of microgrid by virtual moment of inertia and damping [1-4].

When VSG is connected to the medium or low voltage power grid, the connection point is usually at the end of the grid. The power grid fault often occurs such as

short-circuit or voltage imbalance. The operation mechanism and output performance of VSG are not only related to the utilization rate of renewable energy generation, but also affecting the safe and stable operation of the power grid. When a symmetrical fault occurs in the power grid, it is easy to lead to overcurrent for traditional VSG. When an asymmetric fault occurs in the power grid, the output current of the traditional VSG may lead to three-phase unbalance. Therefore, the research on the control strategy of VSG under grid fault mode is important for industrial application. At present, the research on the control strategy of VSG under power grid fault mode is not perfect enough [5-9].

In [10], the superconducting fault current limiter (SFCL) is proposed to the VSG. It can fulfill LVRT because it can restrain the fault current. However, the size and economy of the overall system need to be improved due to the addition of SFCL in hardware. In [11], the dynamic voltage support control strategies are discussed to achieve LVRT for single-phase photovoltaic inverters. Nevertheless, the symmetrical and asymmetric faults in three-phase system are not analyzed in detail. In [12], the transient stability of multi-VSGs is improved in the islanding mode. However, the reactive power compensation and negative sequence current balance during LVRT are not fully described.

Therefore, a control strategy of VSG is proposed in the paper which can regulate the current, voltage, virtual reactance, active power and reactive power for power grid fault. The simulation and experimental results show that the design is feasible.

2. SMALL SIGNAL MODEL OF VSG

2.1 Control Diagram of VSG

As shown in Fig. 1, it is the main circuit of VSG. $e_{abc} = [e_a, e_b, e_c]^T$, $u_{abc} = [u_a, u_b, u_c]^T$, $i_{abc} = [i_a, i_b, i_c]^T$ are the voltage of the bridge arm midpoint, output voltage and output current respectively. R_s is the internal resistor of the inverter. L_s is the filter inductor. C_s is the filter capacitor. P_e is the output active power and Q_e is the output reactive power of the inverter. R_{line} is the line resistor. L_{line} is the line inductor [13-14].

As shown in Fig. 2, it is the power control loop block diagram. The modulation voltage of inverter e_{am} , e_{bm} and e_{cm} are composed of two parts. The active power control loop will generate the phase and the reactive power control loop will generate the voltage amplitude of the internal voltage respectively. Where, P_{set} is the active power reference. D_p is the active power-frequency

droop coefficient. ω is the angular frequency of VSG. ω_N is the nominal angular frequency.

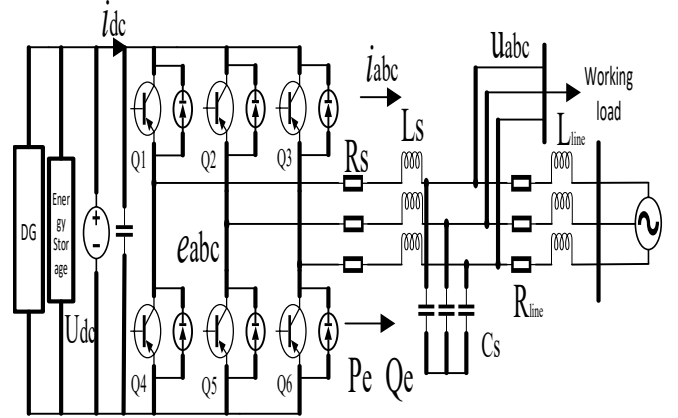


Fig. 1. Main circuit of VSG

And J is the virtual of moment of inertia. K is the reactive power adjustment coefficient. The parameters in the reactive power loop have similar corresponding meanings [15-16].

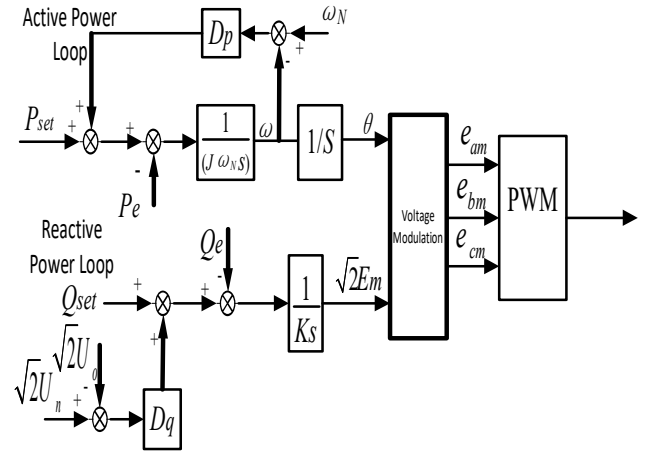


Fig. 2. Power loop control block diagram

2.2 Small Signal Model of VSG

As shown in the equation (1) and (2), it is assumed that the instantaneous value of active power and the instantaneous value of reactive power are equal to their average values in the half period (0.01 s).

$$P_e \approx P_{eT_{line}/2} = \frac{2}{T_{line}} \int_{\frac{T_{line}}{2}} P_e dt \quad (1)$$

$$Q_e \approx Q_{eT_{line}/2} = \frac{2}{T_{line}} \int_{\frac{T_{line}}{2}} Q_e dt \quad (2)$$

$P_{eT_{line}/2}$ — Active power average;

$Q_{eT_{line}/2}$ — Reactive power average;

T_{line} — Period;

Then, the control equation is shown as (3):

$$\left\{ \begin{array}{l} P_{set} + D_p(\omega_N - \omega) - P_e = J\omega_N \frac{d\omega}{dt} \\ \delta = \int (\omega - \omega_N) dt \\ Q_{set} + \sqrt{2}D_q(U_N - U_o) - Q_e = K \frac{d(\sqrt{2}E_m)}{dt} \\ E = K_{PWM}E_m = \frac{U_{in}}{2U_{tri}}E_m \\ P_{eT_{line}/2} = \frac{3EU_N}{X_s} \sin \delta \\ Q_{eT_{line}/2} = \frac{3(E - U_N \cos \delta)E}{X_s} \end{array} \right. \quad (3)$$

Where, δ is the power angle. K_{PWM} is coefficient of the pulse-width modulation (PWM) module. Then, the variable can be described as the sum of the steady state and the small disturbance:

$$\left\{ \begin{array}{l} \omega = \omega_N + \hat{\omega} \\ \delta = \delta_n + \hat{\delta} \\ E_m = E_{mn} + \hat{E}_m \\ E = E_n + \hat{E} \\ P_{eT_{line}/2} = P_{en} + \hat{P}_e \\ Q_{eT_{line}/2} = Q_{en} + \hat{Q}_e \end{array} \right. \quad (4)$$

Where, ω_N , δ_n , E_{mn} , E_n , P_{en} and Q_{en} are the angular frequency, power angle, root mean square (RMS) value of modulating waveform, RMS value of midpoint of the bridge arm, output active power and output reactive power. $\hat{\omega}$, $\hat{\delta}$, \hat{E}_m , \hat{E} , \hat{P}_e , \hat{Q}_e are the small disturbances near the corresponding direct current (DC) working points. When $\sin \hat{\delta} \approx \hat{\delta}$, $\cos \hat{\delta} \approx 1$, $U_o \approx E$, $\hat{\delta} \approx 0$, then

$$\left\{ \begin{array}{l} \hat{P}_{set} - D_p \hat{\omega} - \hat{P}_e = J\omega_N \frac{d\hat{\omega}}{dt} \\ \hat{\delta} = \int \hat{\omega} dt \\ \hat{Q}_{set} - D_q(\sqrt{2}\hat{E}) - \hat{Q}_e = \sqrt{2}K \frac{d\hat{E}_m}{dt} \\ \hat{E} = \frac{U_{in}}{2U_{tri}} \hat{E}_m \\ \hat{P}_e = \frac{3U_N E_n}{X_s} \hat{\delta} \\ \hat{Q}_e = \frac{3}{X_s} (2E_n - U_N) \hat{E} + \frac{3E_n U_N}{X_s} \hat{\delta} \end{array} \right. \quad (5)$$

When $D_{q1} = U_{in}D_q/(2U_{tri})$, the Laplace transformation of equation (5) is:

$$\left\{ \begin{array}{l} \hat{\omega}(s) = \frac{\hat{P}_{set}(s) - \hat{P}_e(s)}{J\omega_N s + D_p} \\ \hat{\delta}(s) = \frac{\hat{\omega}(s)}{s} \\ \hat{E}_m(s) = \frac{\hat{Q}_{set}(s) - \hat{Q}_e(s)}{\sqrt{2}(Ks + D_{q1})} \\ \hat{E}(s) = \frac{U_{in}}{2U_{tri}} \hat{E}_m(s) \\ \hat{P}_e(s) = \frac{3U_N E_n}{X_s} \hat{\delta}(s) + \frac{3U_N}{X_s} \delta_n \hat{E}(s) \\ \hat{Q}_e(s) = \frac{3}{X_s} (2E_n - U_N) \hat{E}(s) + \frac{3E_n U_N}{X_s} \delta_n \hat{\delta}(s) \end{array} \right. \quad (6)$$

According to equation (6), the power-frequency small signal model of VSG in the Laplace domain can be described as shown in Fig. 3.

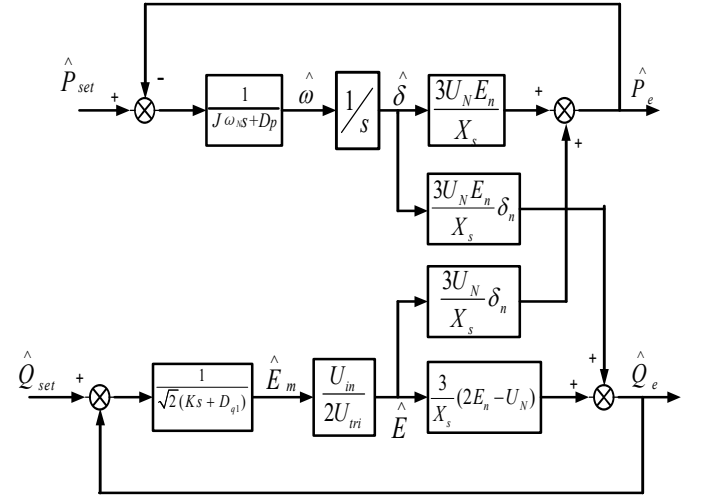


Fig. 3. Small Signal Power loop control block diagram

As shown in Fig. 3, there is coupling between the active power loop and the reactive power loop.

3. LVRT UNDER GRID FAULT MODE

3.1 Restrain Steady and Transient Fault Current

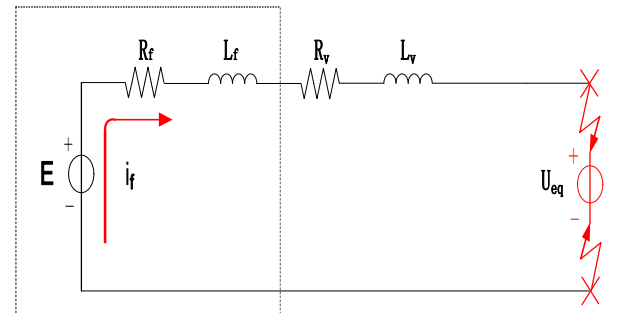


Fig. 4. Equivalent circuit in power grid fault mode

As shown in Fig. 4, it is the equivalent circuit in power grid fault mode. Where, R_f is the equivalent resistor of VSG. L_f is the equivalent inductor of VSG. R_v is the virtual resistor. L_v is the virtual inductor. U_{eq} is the voltage of short-circuit point. E is output voltage of VSG. Then, the steady current $I(\infty)$ and the current at the moment of fault I_{0+} can be calculated as shown in the equation (7) and (8).

$$I(\infty) = \frac{E - U_{eq}(0_+)}{(R_f + R_v) + j(X_f + X_v)} \quad (7)$$

$$I_{0+} = \frac{E - U_{eq}(0_-)}{(R_f + R_v) + j(X_f + X_v)} \quad (8)$$

In the equation (7) and (8), $U_{eq}(0_-)$ and $U_{eq}(0_+)$ are the voltage of short-circuit point before and after 0 second. E depends on the power loop which the adjustment procedure is slow. $U_{eq}(0_+)$ and $U_{eq}(0_-)$ depend on the unpredictable short-circuit point. Therefore, the steady and transient current can be restrained by adjusting the virtual impedance to be $(R_v + jX_v) \gg (R_f + jX_f)$.

From equation (3), the coupling coefficient of active power P can be defined as k_P . And the coupling coefficient of reactive power Q can be defined as k_Q .

$$k_P = \frac{\frac{\partial P}{\partial E}}{\frac{\partial P}{\partial \delta}} = \frac{(sL_v + R_v) \cos \delta + X_v \sin \delta}{-(sL_v + R_v) E \sin \delta + X_v E \cos \delta} \quad (9)$$

$$k_Q = \frac{\frac{\partial Q}{\partial \delta}}{\frac{\partial Q}{\partial E}} = \frac{-(sL_v + R_v) E \cos \delta + X_v E \sin \delta}{-(sL_v + R_v) \sin \delta + X_v \cos \delta} \quad (10)$$

The power coupling coefficient k can be defined as equation (11).

$$k = \frac{k_P}{k_Q} = \frac{R_v \cos \delta + X_v \sin \delta}{-R_v \sin \delta + X_v \cos \delta} \quad (11)$$

The value of the virtual resistance R_v and the virtual reactance X_v can be derived when the power coupling coefficient k is minimum.

The virtual reactance X_v can be calculated by the equation (12).

$$L_v = \frac{X_v}{\omega_n} \quad (12)$$

Where, ω_n is the grid rated angular frequency.

As shown in Fig. 5, it is the corresponding relationship between the power coupling coefficient k and the virtual resistance R_v and virtual reactance X_v .

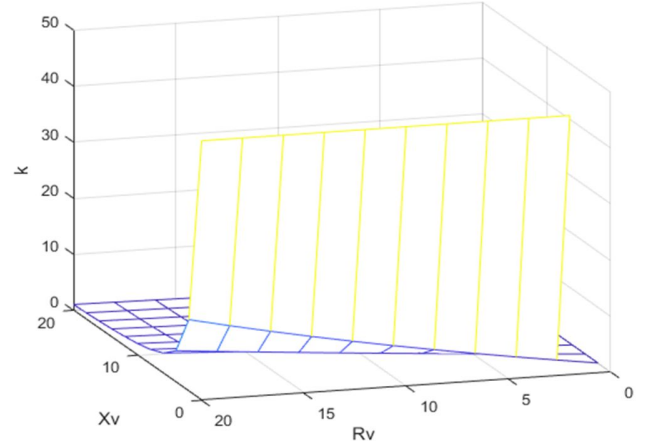


Fig. 5 Power coupling coefficient k

The negative sequence current reference value is set to be zero for the negative sequence current control loop as shown in Fig. 6. Where, the description of the symbols is shown in Table 1.

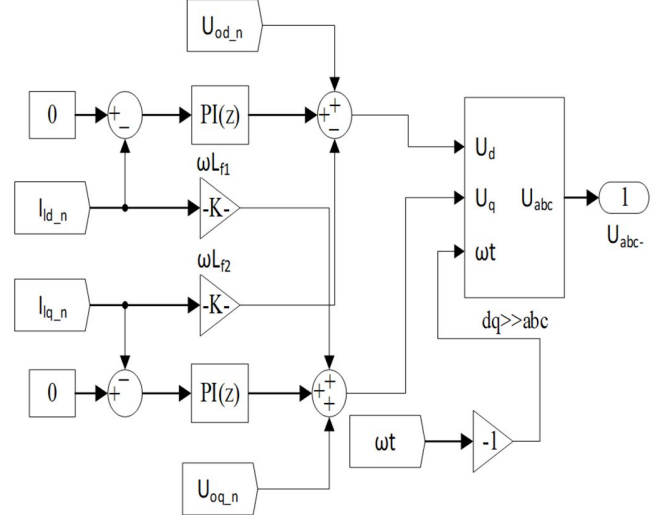


Fig. 6 Negative Sequence Current Control

It is necessary to separate positive and negative sequence components for both voltage and current before control. Therefore, the second order generalized integrator (SOGI) is proposed to separate the positive and negative sequences as shown in Fig. 7. The advantage of SOGI is that it has good filtering characteristics while separating positive and negative sequences.

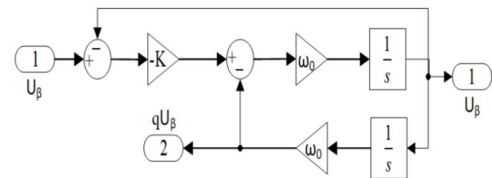


Fig. 7 Second Order Generalized Integrator

3.2 Three-phase balance current adjustment

When an asymmetrical fault occurs in the power grid, the VSG is required to not disconnect from the power grid and the output current to maintain three-phase balance. Therefore, the output current control is divided into the positive sequence control and negative sequence control respectively. The positive sequence current control maintains the original control strategy.

3.3 Active and Reactive Power Regulation

When the voltage of connection point drops because of power grid failure, VSG is required to supply extra reactive power to the grid to support the power grid voltage. The deeper the grid voltage drops, the greater the reactive power required to be supplied for the grid as shown in the equation (13).

$$\Delta Q = K_u Q_n * \frac{\Delta U}{U_n} \quad (13)$$

Where, ΔQ is the reactive power variation and ΔU is the voltage variation. K_u is the proportional coefficient.

As shown in Fig. 8 (a), the output active power will decrease because the voltage drops during the power grid fault. According to the law of equal area, the whole system will be unstable if the acceleration area is larger than the maximum deceleration area. Therefore, it is necessary to reset the reference value of the active power by equation (14) and (15). As shown in Fig. 8 (b), it can not only reduce the acceleration area, but also increase the maximum deceleration area.

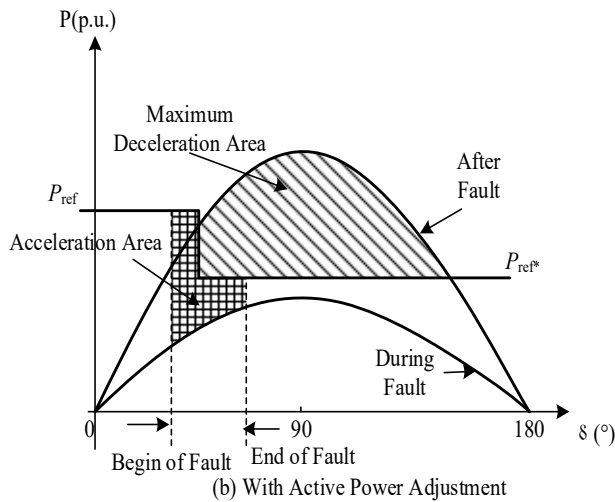
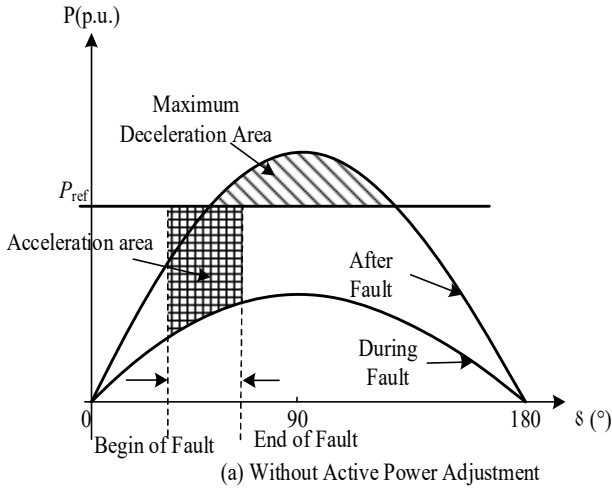


Fig. 8 P- δ curve

$$\Delta P \geq P_n - \sqrt{(P_n^2 + Q_n^2) - (Q_n + \Delta Q)^2} \quad (14)$$

$$P_{ref*} = P_{ref} - \Delta P \quad (15)$$

Where, P_{ref} is the original reference value of active power and P_{ref*} is the modified reference value of active power during the power grid fault.

4. SIMULATION AND EXPERIMENT

The VSG model based on MATLAB is built for simulation to verify the effectiveness of the design. The LVRT is validated in the case of single-phase, two-phase and three-phase power grid faults. The parameters of the model are shown in Table 2.

TABLE 2: PARAMETERS OF SIMULATION MODEL

Parameter	Value	Parameter	Value
Rated frequency	50 Hz	Filter inductance	$2 \cdot 10^{-3}$ H
Switching frequency	10 KHz	Line capacitance	$5 \cdot 10^{-6}$ F
Rated AC voltage	380 V	Filter resistance	0.02 Ω
DC voltage	700 V	Rated active power	9 KW
Virtual moment of inertial	0.1	Virtual damping	15

The whole simulation time is 1.7 S. During 0-0.5 S, the power grid voltage is normal. The fault in power grid occurs from 0.5 S to 1.2 S. And the fault is cleared from 1.2 S.

4.1 Single-phase Fault

As shown in Fig. 9 and Fig. 10, it is the waveform of the single-phase fault under LVRT and traditional VSG mode. The single-phase voltage drops to 60% of the rated voltage. The active power reference is set to be 9 KW. And the reactive power reference is set to be 0 KVar. In the traditional VSG mode, the output current is unbalance and is larger than normal value. The active power does not change much during the fault. In LVRT mode, the output current is balance and the fault current is less than normal value. The active power decreases and the reactive power increases during the fault. When the single-phase fault is over, the active power and reactive power restore to be the normal value.

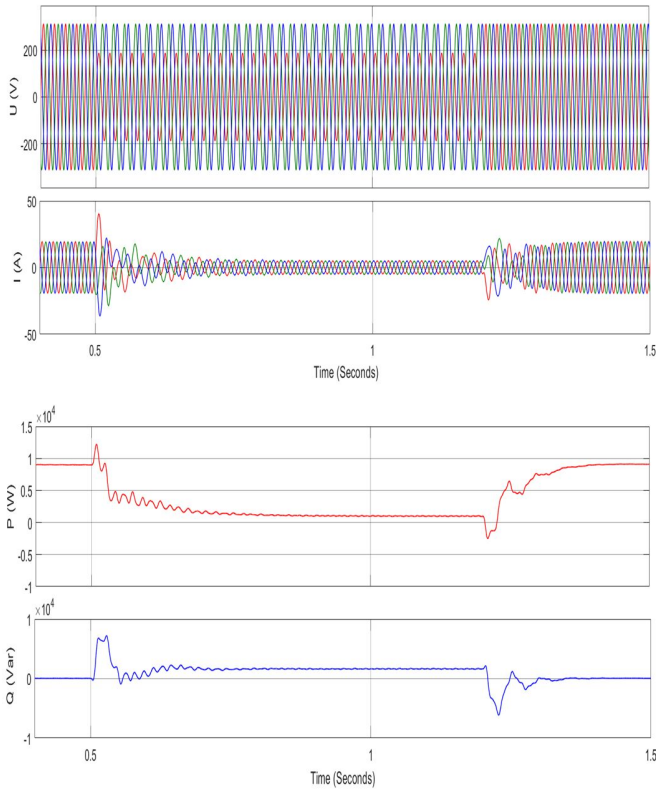


Fig. 9 Single-phase fault of LVRT mode

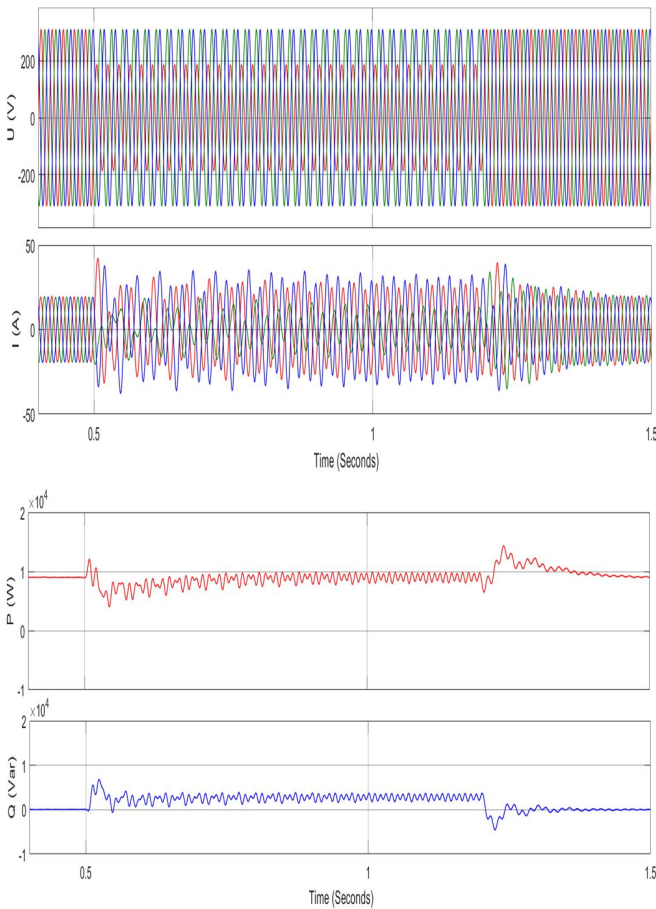


Fig. 10 Single-phase fault of traditional VSG mode

4.2 Two-phase Fault

As shown in Fig. 11 and Fig. 12, it is the waveform of the two-phase fault under LVRT and traditional VSG mode. The two-phase voltage drops to 40% of the rated voltage. The active power reference is set to be 9 KW. And the reactive power reference is set to be 0 KVar. Compared with the traditional mode, the output current is balance and the fault current is less than normal value In LVRT mode.

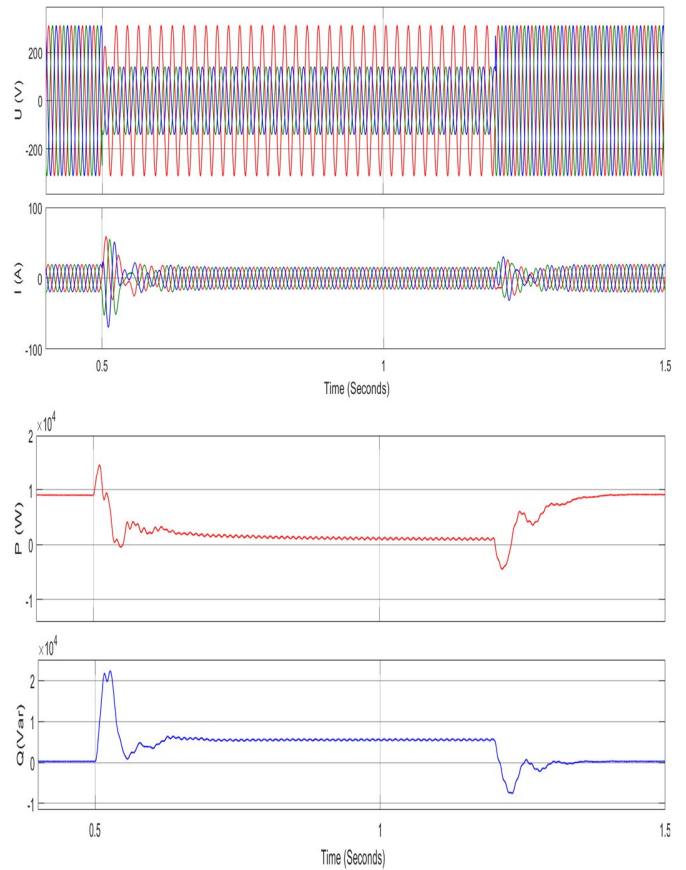
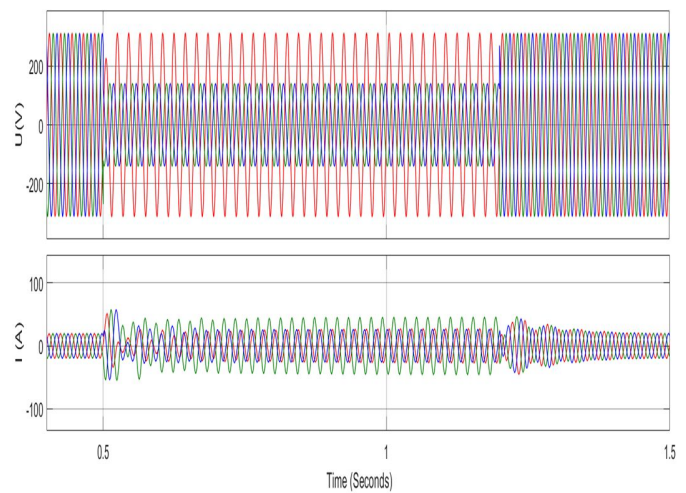


Fig. 11 Two-phase fault of LVRT VSG mode



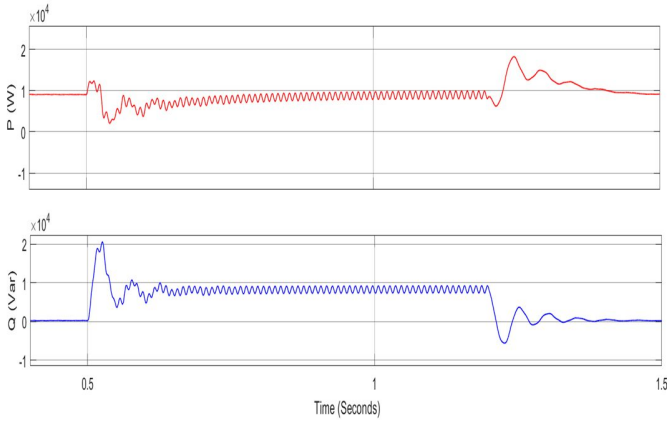


Fig. 12 Two-phase fault of LVRT mode

4.3 Three-phase Fault

As shown in Fig. 13 and Fig. 14, it is the waveform of the three-phase fault under LVRT and traditional VSG mode. The three-phase voltage drops to 60% of the rated voltage. The active power reference is set to be 9 KW. And the reactive power reference is set to be 0 KVar. In the traditional VSG mode, the output current is larger than the current in LVRT. The active power does not change much during the fault in traditional VSG mode. And the active power decreases during the fault in LVRT mode.

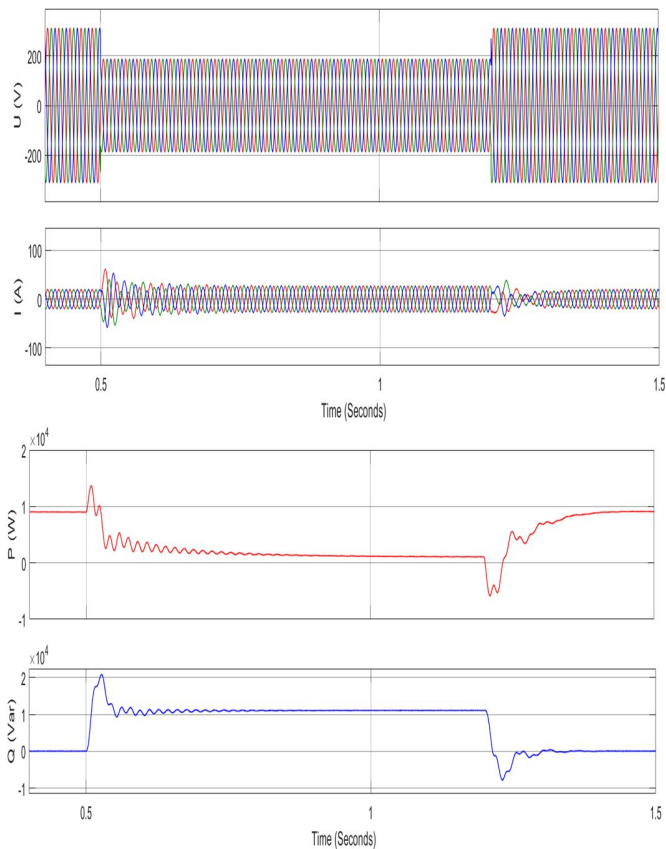


Fig. 13 Three-phase fault of LVRT mode

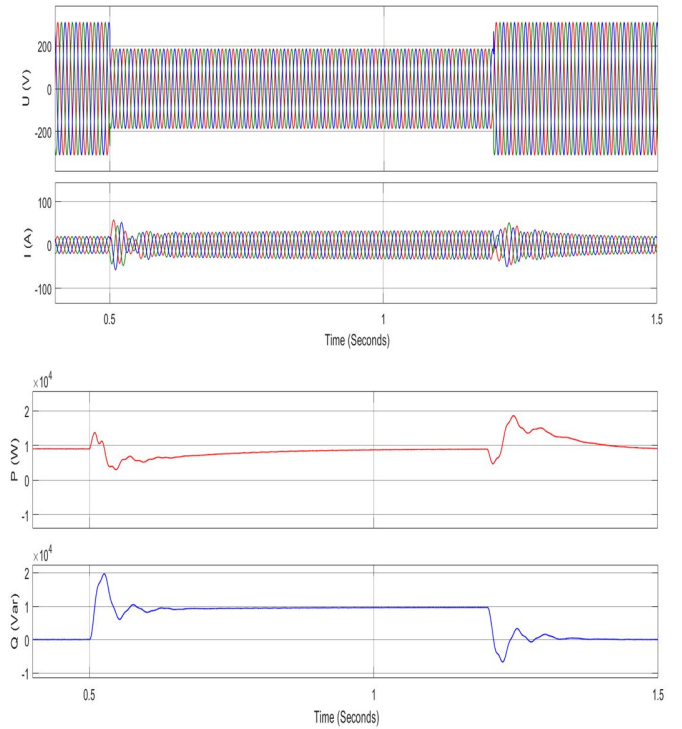


Fig. 14 Three-phase fault of traditional VSG mode

4.4 Experiment

An experiment platform is built to verify the effectiveness of the LVRT control strategy. The DC power supply is Agilent N8955A. The three-phase inverter is YXPHM-TP210B-II. The AC power supply is Chroma programmable AC source 61512 which can emulate the power grid fault. The controller is YXSPACE sp2000. The experimental results under asymmetric and symmetric are shown as Fig. 15 and Fig.16. When the phase A, B or C voltage drops, the output current is stable, balance and not overcurrent. The reactive power increases and the active power decreases during the grid fault. The active power and reactive power of VSG restore to be normal after the grid fault is over.

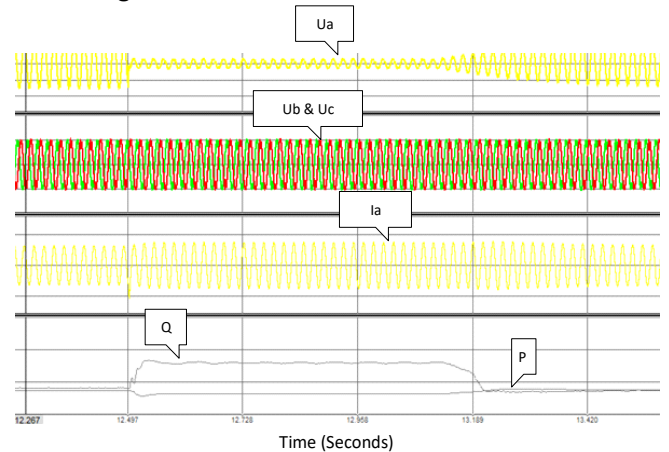


Fig. 15 20% sag of single-phase fault

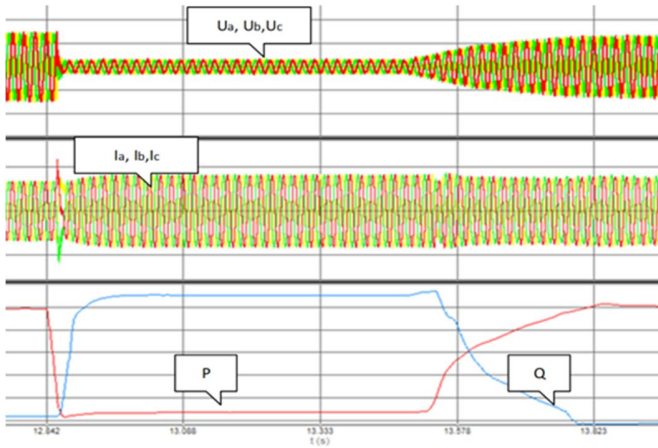


Fig. 16 20% sag of three-phase fault

4.5 Results and Discussion

As shown from Fig. 9 to Fig. 15, the waveforms in LVRT mode have been improved compared with the traditional VSG mode. In the traditional VSG mode, the output current is unbalance and is larger than the normal value. The active power and reactive power do not change much during the fault. In LVRT mode, the output current is balance and the fault current is less than the normal value. The active power decreases and the reactive power increases during the fault. When the symmetrical or asymmetric fault is over, the active power and reactive power can restore to be the normal value in time.

5. CONCLUSIONS

A LVRT control strategy of VSG is proposed in detail in the paper. The virtual reactance is designed to restrain the transient and steady fault current. The negative sequence current control is designed to eliminate the unbalance of output current. The reactive and active power is designed to support the power grid voltage and improve the stability. The simulation and experiment result shows that the control strategy of VSG under power grid fault mode is feasible and effective.

ACKNOWLEDGEMENTS

This work was supported by the Ningbo Science Foundation of China (Grant no. 202003N4182) and the title is Frequency Response Analysis of a Modular Multilevel Power Converter for Multi-terminal HVDC Applications.

REFERENCE

- [1] W. Wang, L. Jiang, Y. Cao and Y. Li, "A Parameter Alternating VSG Controller of VSC-MTDC Systems for Low Frequency Oscillation Damping," in IEEE Transactions on Power Systems, vol. 35, no. 6, pp. 4609-4621, Nov. 2020, doi: 10.1109/TPWRS.2020.2997859.
- [2] J. Chen and T. O'Donnell, "Parameter Constraints for Virtual Synchronous Generator Considering Stability," in IEEE Transactions on Power Systems, vol. 34, no. 3, pp. 2479-2481, May 2019, doi: 10.1109/TPWRS.2019.2896853.
- [3] L. Zhou et al., "Impedance-Based Harmonic Current Suppression Method for VSG Connected to Distorted Grid," in IEEE Transactions on Industrial Electronics, vol. 67, no. 7, pp. 5490-5502, July 2020, doi: 10.1109/TIE.2019.2934084.
- [4] Z. Qu, J. C. -H. Peng, H. Yang and D. Srinivasan, "Modeling and Analysis of Inner Controls Effects on Damping and Synchronizing Torque Components in VSG-Controlled Converter," in IEEE Transactions on Energy Conversion, vol. 36, no. 1, pp. 488-499, March 2021, doi: 10.1109/TEC.2020.3010049.
- [5] Q. Xu, T. Dragicevic, L. Xie and F. Blaabjerg, "Artificial Intelligence-Based Control Design for Reliable Virtual Synchronous Generators," in IEEE Transactions on Power Electronics, vol. 36, no. 8, pp. 9453-9464, Aug. 2021, doi: 10.1109/TPEL.2021.3050197.
- [6] X. Zhang et al., "A Grid-Supporting Strategy for Cascaded H-Bridge PV Converter Using VSG Algorithm With Modular Active Power Reserve," in IEEE Transactions on Industrial Electronics, vol. 68, no. 1, pp. 186-197, Jan. 2021, doi: 10.1109/TIE.2019.2962492.
- [7] W. Wu et al., "Sequence Impedance Modeling and Stability Comparative Analysis of Voltage-Controlled VSGs and Current-Controlled VSGs," in IEEE Transactions on Industrial Electronics, vol. 66, no. 8, pp. 6460-6472, Aug. 2019, doi: 10.1109/TIE.2018.2873523.
- [8] C. Li, Y. Yang, N. Mijatovic and T. Dragicevic, "Frequency Stability Assessment of Grid-Forming VSG in Framework of MPME With Feedforward Decoupling Control Strategy," in IEEE Transactions on Industrial Electronics, vol. 69, no. 7, pp. 6903-6913, July 2022, doi: 10.1109/TIE.2021.3099236.
- [9] M. Zhao, H. Yin, Y. Xue, X. -P. Zhang and Y. Lan, "Coordinated Damping Control Design for Power System With Multiple Virtual Synchronous Generators Based on Prony Method," in IEEE Open Access Journal of Power and Energy, vol. 8, pp. 316-328, 2021, doi: 10.1109/OAJPE.2021.3104755.
- [10] L. Chen et al., "Investigation of Flux-Coupling-Type SFCLs for Enhancing Interconnectivity of Multiple

Microgrid Clusters Under Fault Conditions," in IEEE Transactions on Applied Superconductivity, vol. 31, no. 8, pp. 1-7, Nov. 2021, Art no. 5603407, doi: 10.1109/TASC.2021.3094455.

[11] M. A. Khan, A. Haque and V. S. B. Kurukuru, "Dynamic Voltage Support for Low-Voltage Ride-Through Operation in Single-Phase Grid-Connected Photovoltaic Systems," in IEEE Transactions on Power Electronics, vol. 36, no. 10, pp. 12102-12111, Oct. 2021, doi: 10.1109/TPEL.2021.3073589.

[12] M. Choopani, S. H. Hosseinian and B. Vahidi, "New Transient Stability and LVRT Improvement of Multi-VSG Grids Using the Frequency of the Center of Inertia," in IEEE Transactions on Power Systems, vol. 35, no. 1, pp. 527-538, Jan. 2020, doi: 10.1109/TPWRS.2019.2928319.

[13] X. Liang, C. Andalib-Bin-Karim, W. Li, M. Mitolo and M. N. S. K. Shabbir, "Adaptive Virtual Impedance-Based Reactive Power Sharing in Virtual Synchronous Generator Controlled Microgrids," in IEEE Transactions on Industry Applications, vol. 57, no. 1, pp. 46-60, Jan.-Feb. 2021, doi: 10.1109/TIA.2020.3039223.

[14] K. Shi, W. Song, H. Ge, P. Xu, Y. Yang and F. Blaabjerg, "Transient Analysis of Microgrids With Parallel Synchronous Generators and Virtual Synchronous Generators," in IEEE Transactions on Energy Conversion, vol. 35, no. 1, pp. 95-105, March 2020, doi: 10.1109/TEC.2019.2943888.

[15] L. Huang, H. Xin and Z. Wang, "Damping Low-Frequency Oscillations Through VSC-HVdc Stations Operated as Virtual Synchronous Machines," in IEEE Transactions on Power Electronics, vol. 34, no. 6, pp. 5803-5818, June 2019, doi: 10.1109/TPEL.2018.2866523.

[16] O. Babayomi, Z. Li and Z. Zhang, "Distributed secondary frequency and voltage control of parallel-connected vscs in microgrids: A predictive VSG-based solution," in CPSS Transactions on Power Electronics and Applications, vol. 5, no. 4, pp. 342-351, Dec. 2020, doi: 10.24295/CPSSPEA.2020.00028.